International Journal of Fluid Machinery and Systems
Vol. 3, No. 3, July-September 2010

DOI: 10.5293/IJFMS.2010.3.3.211
ISSN (Online): 1882-9554

Original Paper

Unsteady Swirling Flows Arising in Straight Tubes

Hiromu Tsurusaki

Department of Mechanical Systems Engineering, Fukuyama University,
Fukuyama, Hiroshima 729-0292, Japan

Abstract

The objective of this study is to clarify the occurrence of the high-speed mode of unsteady swirling flows in straight tubes. The unsteady flows generated in the tube were measured by means of a semiconductor-type pressure transducer and an FFT analyzer. The high-speed mode measured has rotational speed which is approximately equal to or higher than the peripheral velocity of the swirling flow. The unsteady flow is due to cell rotation in the circumferential direction of the tube. The occurrence of the high-speed mode was confirmed, and the characteristics (rotational speed, pressure amplitude, and phase) of this mode were clarified. In order to understand the measured unsteady flows, the three dimensional vortex core profiles were discussed based on the distributions of the pressure amplitude and phase.

Keywords: Unsteady Flow, Swirling Flow, Whirling Vortex, Pressure Fluctuation, Rotating stall.

1. Introduction

Fluid machines often include swirling flows in their flow channels. Examples of such machinery and flow channels are a swirl burner that handles combustion gas having swirl velocity, a draft tube of a hydraulic turbine, a vaneless diffuser of mixed-flow-type turbomachinery, and a Ranque-Hilsch tube used as a cooling device. In these flow channels, various types of unsteady flows often arise due to the unstable swirling flow (Tsurusaki, H. [1]- Kurosaka, M. [5]). The present author found that unsteady flows occur in a mixed-flow-type vaneless diffuser system (Tsurusaki, H. [1]) that is similar to the Ranque-Hilsch tube (Kurosaka, M. [5]). Two kinds of unsteady flows, low- and high-speed modes, are generated in the flow channel. The experiment clarified that the origin of the low-speed mode is the vaneless diffuser; the origin of the high-speed mode is assumed to be in the inlet tube used in the test rig. The high-speed mode has a rotational speed higher than the swirl velocity of the inflow given to the flow channel. The present study was carried out in order to confirm the occurrence of the high-speed mode in the straight tube. The experimental apparatus was constructed from a swirl flow generator and a straight tube, and air was used as the working fluid.

2. Experimental Apparatus

Figure 1(a) shows the experimental apparatus used in the present study. Pressurized air is introduced into the tube through eight jet holes of a swirl flow generator (flow rate Q_0). A portion of the inflow is extracted (flow rate Q_1) through an exhaust tube in order to control the outflow ($Q=Q_0-Q_1$) of the tube. The exit of the tube is opened to the atmosphere.

Space-averaged axial velocity v in the direction of the tube exit is obtained from $v=4Q/\pi d_s^2$, where d_s (=80 mm) is tube diameter. Swirl velocity u of the inflow is obtained from $u=u_j\sin\theta=(4Q_0/8\pi d_j^2)\sin\theta$, where d_j (=8.6 mm) is jet diameter and θ (=60 degrees) is the jet angle as measured from the normal of the tube wall.

Measurements were carried out for four kinds of tubes in which nondimensional tube lengths L/d_s=2.03, 4.54, 7.04, and 9.55, where L is the axial distance between the jet holes and the tube exit. Except for the case of L/d_s=2.03, extension tubes were inserted between the swirl flow generator and the straight tube shown in Fig. 1(a).

The details of the measurement point are shown in Fig. 1(b). The frequency response of the pressure transducer with an adapter was estimated before the experiment was carried out (see Appendix).

Figure 1(c) shows the experimental apparatus used in the measurement of pressure distributions in a cross section located 0.5 d_s apart from the tube exit. Pressure waves were measured at the center of the disk (diameter=2.5d_s) set perpendicularly to the tube axis. A pressure transducer was set at the center of the disk, and another pressure transducer was fixed on the tube wall. The disk was traversed perpendicularly to the tube axis in order to measure the pressure waves at the eight measurement points located in the equal interval from r/d_s=0.0625 to r/d_s=0.5.

Received October 20 2009; revised June 25 2010; accepted for publication June 28 2010: Review conducted by Prof. Hyung Hee Cho. (Paper number O09048)
Corresponding author: Hiromu Tsurusaki, Professor, htsu@fume.fukuyama-u.ac.jp

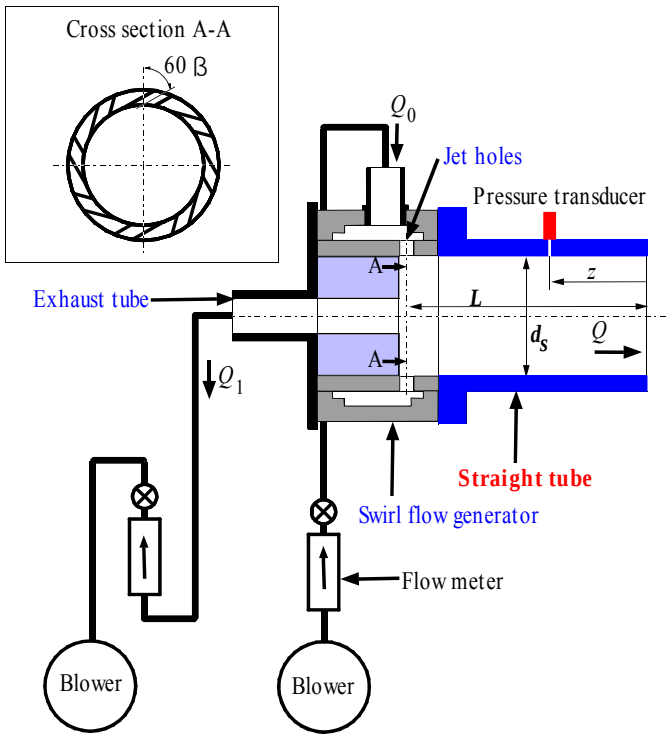

Fig. 1(a) Experimental apparatus

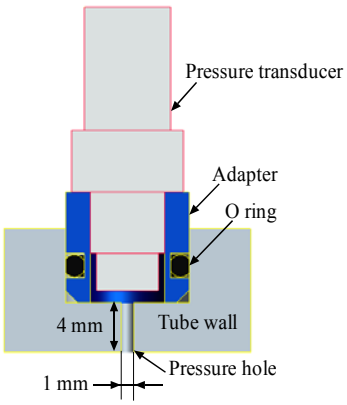

Fig. 1(b) Details of measurement point (Installation of pressure transducer with adapter)

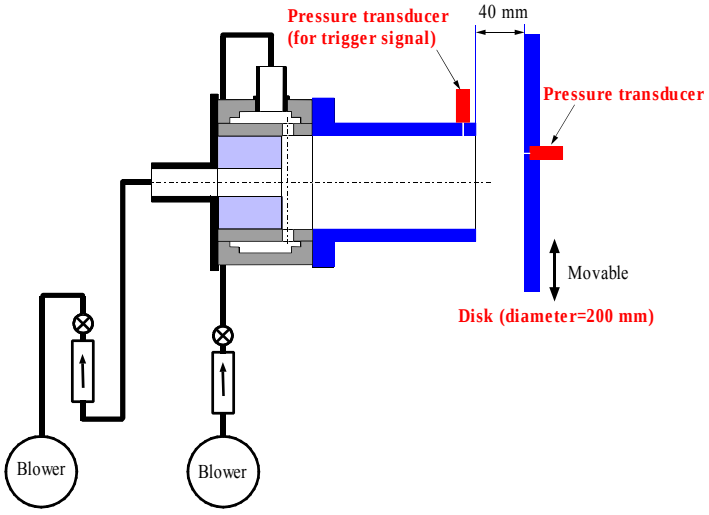

Fig. 1(c) Measurement of pressure distributions in a cross section outside the tube (L/d_s=4.54)

3. Measurement Method

The pressure fluctuations were measured by means of semiconductor-type pressure transducers. Figures 2(a), 2(b), and 2(c) show the measurement systems of the frequency spectra, phase difference, and pressure waves in a cross section outside the tube, respectively.

Frequency spectra of the pressure fluctuations were measured at a measurement point z/d_s =0.875 on the tube wall, where z (see Fig. 1(a)) is the axial distance between the measurement point and the tube exit. A frequency spectrum was obtained from the ensemble average of 128 spectra by means of an FFT analyzer. The sampling frequency and frequency resolution of the FFT analyzer were 1280 Hz and 1.25 Hz, respectively.

A phase difference δ (degrees) between two points located γ (degrees) apart on the tube wall at z/d_s=0.875 was measured by means of a function (ensemble average of 128 cross spectra) of the FFT analyzer. The number of cells λ of the unsteady flow was determined from $\lambda=\delta/\gamma$. The rotational speed of the cell f_r was obtained from $f_r=f/\lambda$, where f is the fundamental frequency of pressure fluctuation.

The axial distribution of the pressure amplitude and phase were measured at measurement points located axially on the tube

wall by means of the FFT analyzer.

The pressure waves were measured on the disk set perpendicularly to the tube axis. A pressure transducer was set at the center of the disk, and another pressure transducer was fixed on the tube wall at z/d_s=0.125. The output of the pressure transducer on the tube wall was filtered in order to obtain a signal having a fundamental frequency, and the filter output was input as a trigger signal to the FFT analyzer. A pressure wave on the disk was obtained from the ensemble average of 256 pressure waves. The disk was traversed perpendicularly to the tube axis in order to measure the pressure waves at the eight measurement points located in the equal interval from r/d_s=0.0625 to r/d_s=0.5. The pressure distribution was obtained by developing the pressure data in the circumferential direction of the disk.

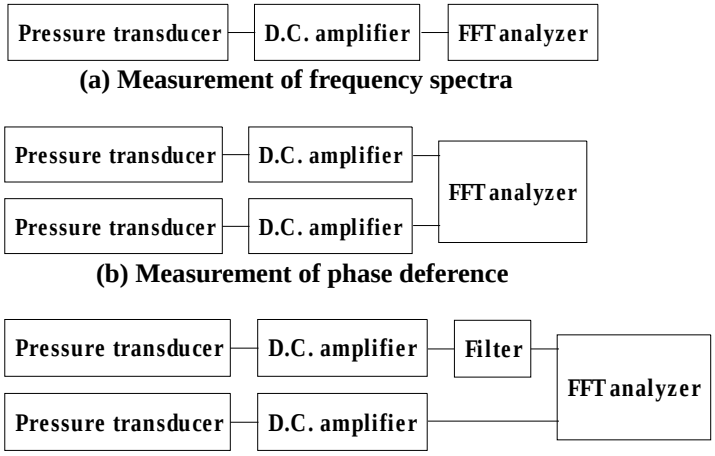

(a) Measurement of frequency spectra

(b) Measurement of phase deference

(c) Measurement of pressure waves

Fig. 2 Measurement systems of pressure fluctuations

4. Experimental Results and Discussion

4.1 Generation of unsteady flows

Figure 3 shows the frequency spectra of the pressure fluctuations measured at u=21.8 m/s for the tube in which L/d_s=4.54. Unsteady flow having a fundamental frequency of 82.5 Hz was generated at v/u=0.107. The amplitude and fundamental frequency of the pressure fluctuation increased with decreasing v/u. The number of cells was 1 at all values of v/u.

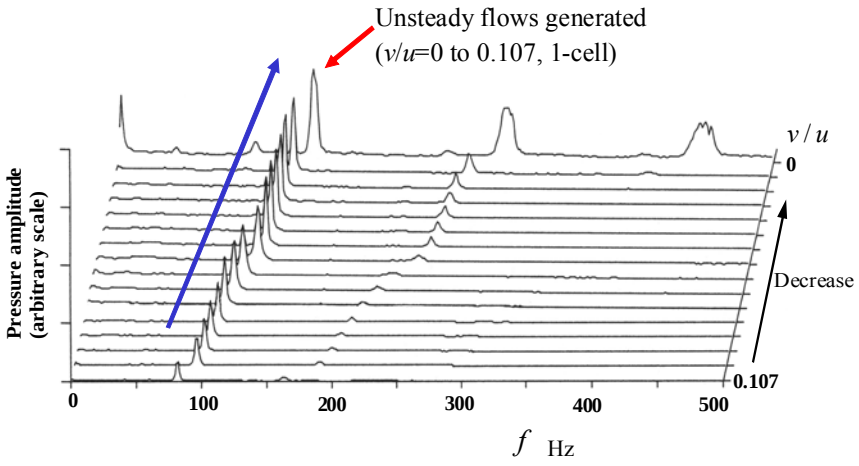

Fig. 3 Frequency spectra of pressure fluctuations

4.2 Nondimensional rotational speed of the cell and pressure amplitude

The measurements were carried out under conditions where v/u is between 0 and 0.107 for four kinds of tubes of nondimensional tube lengths L/d_s=2.03, 4.54, 7.04, and 9.55. At v/u=0, the flow rate of the inflow is completely extracted from the exhaust tube. In contrast, no flow rate is extracted at v/u=0.107.

In many cases, the number of measured cells was 1. Unsteady flows of 2-cell mode were measured only in the case where L/d_s=2.03 and v/u=0.031-0.107. Figure 4(a) shows changes of the nondimensional rotational speed of the cell $\pi d_s f_r/u$ with the velocity ratio v/u in the case of 1-cell. A universal relationship between f_r and v was confirmed to be obtained when these parameters are normalized with respect to u (Tsurusaki, H. [1]). The nondimensional rotational speed used here is the Strouhal

number used as a parameter of periodic flows. Figure 4(b) shows changes in the nondimensional pressure amplitude $p/\rho u^2$ with v/u, where p is pressure amplitude and ρ is air density. The unsteady flows with 1-cell were measured under the condition $v/u<0.107$. The nondimensional rotational speed and pressure amplitude gradually increase with decreasing v/u, and assume maximum values near $v/u=0$. At an arbitrary value of v/u, nondimensional rotational speed assumes a large value when the short tube is used. The reason for this result is that the swirl velocity is decreased by the viscous stress on the tube wall, and the space-averaged swirl velocity in the short tube is greater than that in the long tube. Therefore, the nondimensional rotational speed for the short tube is greater than that for the long tube.

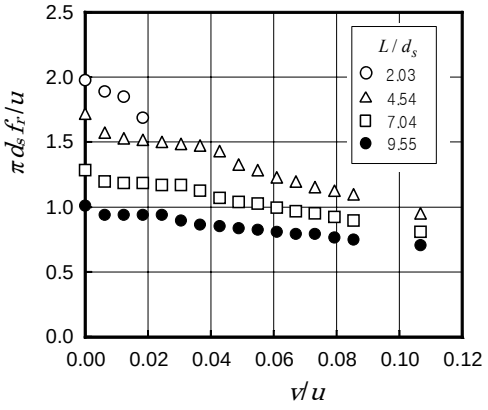

Fig. 4(a) Nondimensional rotational speed (1-cell)

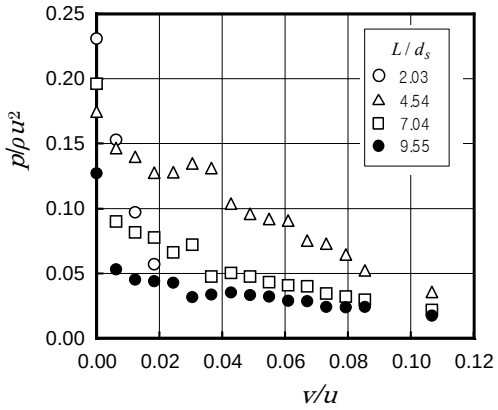

Fig. 4(b) Nondimensional prssure amplitude (1-cell)

The measured results confirmed that the unsteady flow corresponding to the high-speed mode in the previous experiment (Tsurusaki, H. [1]) was generated in the tested tubes. In the previous experiment, the length of the straight tube excluding the mixed-flow-type vaneless diffuser is L/d_s=3.5. Table 1 compares the nondimensional rotational speeds measured in the present and previous experiments. At v/u=0.08, the two values are close to each other, but at v/u=0 the present experiment gives a considerably large value. The high-speed mode having a nondimensional rotational speed higher than 1.0 appeared in the straight tube. The present experiment clarified that the origin of the high-speed mode in the previous experiment was the straight tube.

Table 1 Comparison of measured nondimensional rotational speeds of the cell

	v/u=0.08	v/u=0
Previous experiment (L/d_s=3.5, 1-cell)	0.75－1.0	1.0－1.2
Present experiment (L/d_s=4.54, 1-cell)	About 1.1	About 1.7

4.3 Axial distribution of the pressure amplitude and phase

The measurements were carried out under the conditions of v/u=0.079, 0.012, and 0. Figures 5(a) and 5(b) show the axial distributions of the nondimensional pressure amplitude and phase δ (phase lead) at v/u=0.079, respectively. The nondimensional pressure amplitude is relatively small within the range of $z/d_s>2.5$, where z is the axial distance between the measurement point and the tube exit. The nondimensional pressure amplitude increases within the range of z/d_s=2.5-0.8, assumes a maximum value near z/d_s=0.8, and decreases in the direction of the tube exit (z/d_s=0). In the case of L/d_s=4.54, the nondimensional pressure amplitude again increases near the tube exit. Within the range of z/d_s=1.5-0, the changes in phase are similar for all values of L/d_s. In the case of L/d_s=9.55, a large change in phase is observed within the range of z/d_s=4.0-2.0; however, the nondimensional pressure amplitude is very small within the same range.

The pressure fluctuations are considered to be caused by the rotation of the region where vorticity is concentrated. A similar phenomenon has been observed in the draft tube of a hydraulic turbine as a whirling vortex (Nishi, M., et al. [2]).

Figures 6(a) and 6(b) show the results measured at v/u=0.012. The nondimensional pressure amplitude is large as compared with that measured at v/u=0.079. In particular, it becomes very large at the tube exit, in spite of that the exit is opened to the atmosphere. The phase distributions are similar to that in the case where L/d_s =9.55 and v/u=0.079.

Figures 7(a) and 7(b) show the results measured at v/u=0. The nondimensional pressure amplitude is large near z/d_s=1.0, and very small at the tube exit except for the case of L/d_s=2.03. The phase is abruptly changed near z/d_s=1.0.

4.4 Consideration on the vortex-core profile

From the axial distributions of the nondimensional pressure amplitude and phase, we can imagine the change of the whirl radius of the vortex core and the diffusion of vorticity. The pressure amplitude measured on the tube wall is considered to be large when the whirl radius (see Fig. 8(a)) of the vortex is large and small when the diffusion of vorticity occurs.

Although the profile of the vortex core was not directly measured, it is discussed by reference to the measured axial distributions of the pressure (Figs. 5(a)-7(b)). The understanding for the present unsteady flows becomes easy by this discussion.

The parameters which express the pressure pattern or vortex-core profile are defined as

$x = (p/\rho u^2)\sin(\delta - \delta_{peak})$,

$y = -(p/\rho u^2)\cos(\delta - \delta_{peak})$,

where δ_{peak} is the phase of the pressure at the peak near z/d_s=0.8. Figures 8(a) and 8(b) show the (x, y, z) coordinate system for the representation of the vortex core profile.

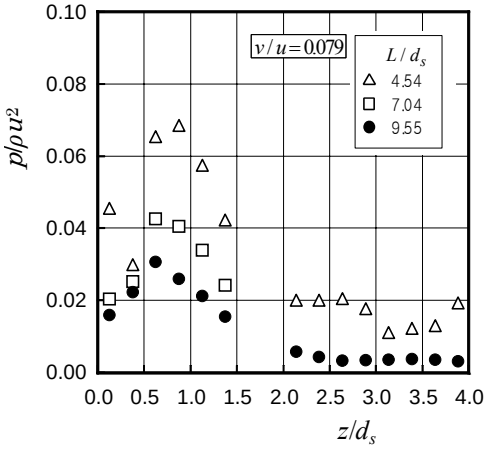

Fig. 5(a) Axial distribution of nondimensional pressure amplitude (*v*/*u*=0.079)

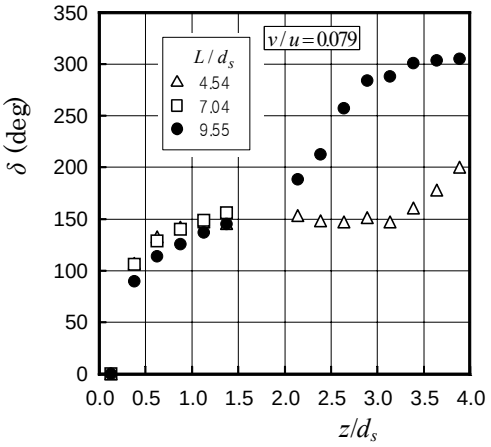

Fig. 5(b) Axial distribution of phase (*v*/*u*=0.079)

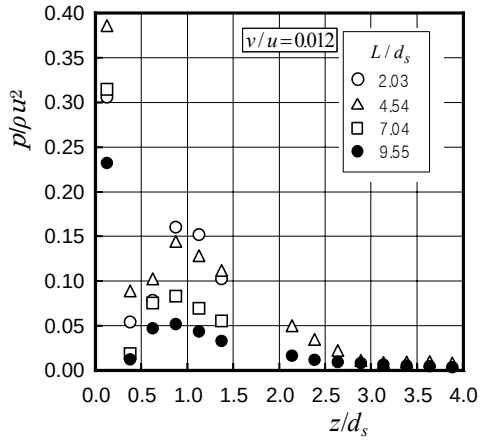

Fig. 6(a) Axial distribution of nondimensional pressure amplitude (*v*/*u*=0.012)

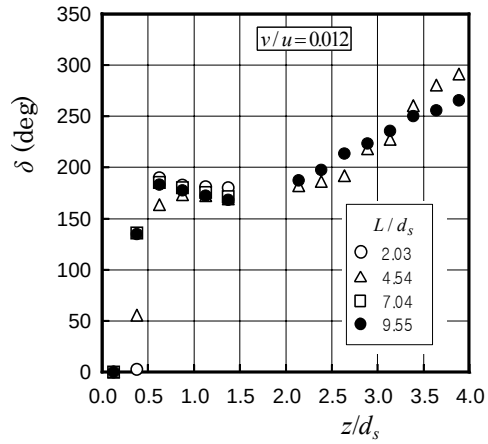

Fig. 6(b) Axial distribution of phase (*v*/*u*=0.012)

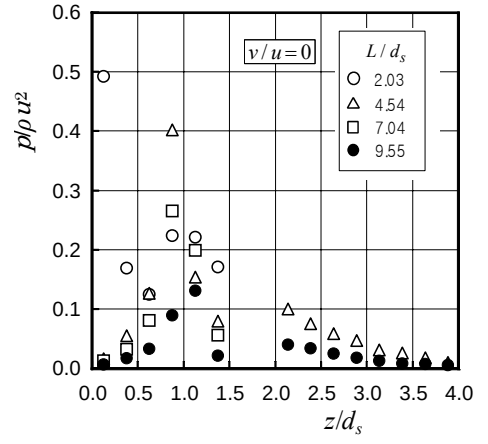

Fig. 7(a) Axial distribution of nondimensional pressure amplitude (*v*/*u*=0)

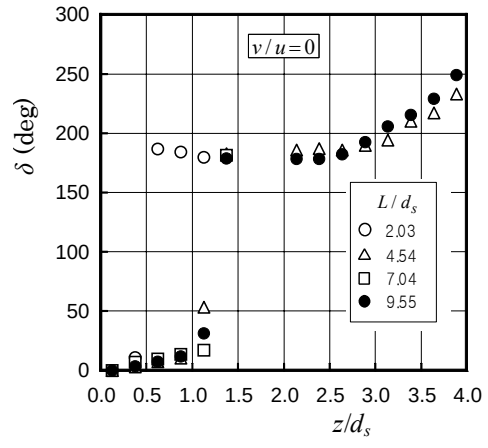

Fig. 7(b) Axial distribution of phase (*v*/*u*=0)

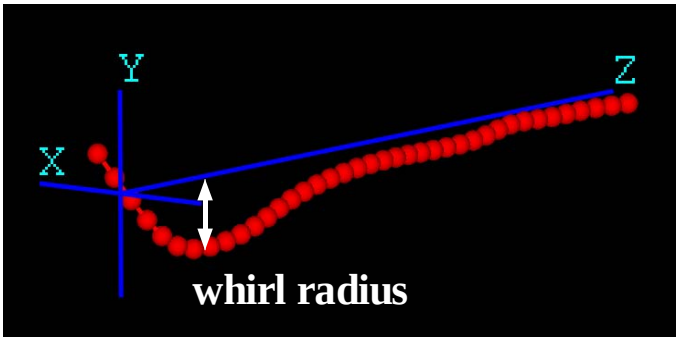

Fig. 8(a) 3-D image of vortex core profile

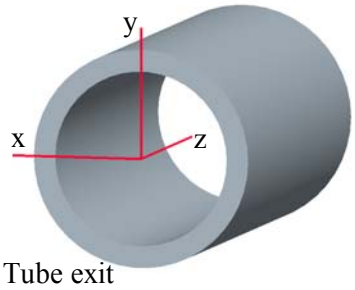

Fig. 8(b) Coordinate system for representation of vortex core profile

Figures 9(a) and 9(b) illustrate the cross sectional view and side view of the pressure pattern, respectively, in the case where L/d_s=4.54 and v/u=0.079. Within the range of z/d_s=4.0-about 1.0 (region R1), the whirl radius of the vortex is increased (absolute value of y is increased) in the direction of the tube exit. The deformation of the vortex core is two-dimensional (2-D deformation). The vortex core rebounds near z/d_s=1.0 and three-dimensional deformation occurs within the range of z/d_s=about 1.0-0 (region R2). The assumed vortex profile is quite different from the spiral vortex observed in the draft tube of the hydraulic turbine (Nishi, M., et al. [2]).

Figures 10(a) and 10(b) illustrate the results at v/u=0.012. Although the pressure amplitudes are very large within the range of z/d_s=about 1.0-0 as compared with that measured at v/u=0.079, a similar pressure pattern is obtained.

Figures 11(a) and 11(b) illustrate the results at v/u=0. The 2-D and 3-D deformations occur within the range of z/d_s=4.0-about 1.0, and the 2-D deformation occurs again within the range of z/d_s=about 1.0-0 after the rebound near z/d_s=1.0. As a result, the pressure amplitude is very small at the tube exit.

These vortex core profiles mentioned above may not be different from those measured directly. However, the characteristics of the present unsteady flows can be easily understood and recognized by this consideration.

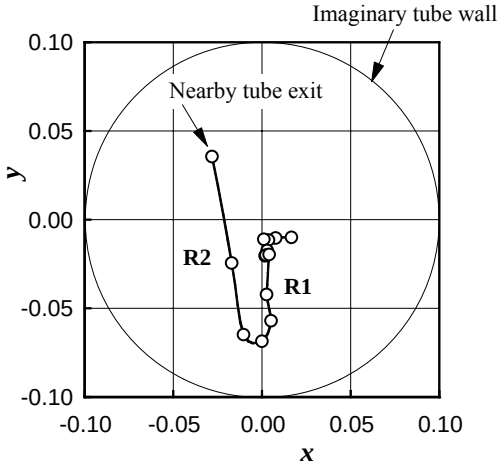

(a) Cross sectional view

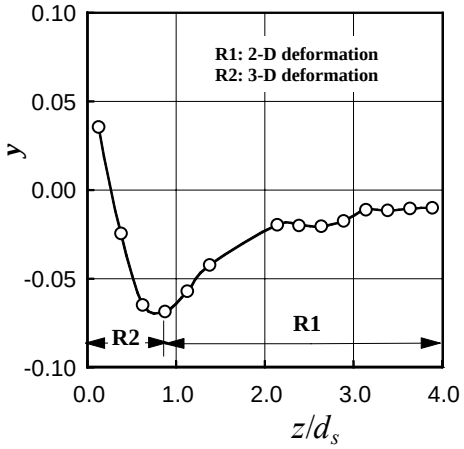

(b) Side view

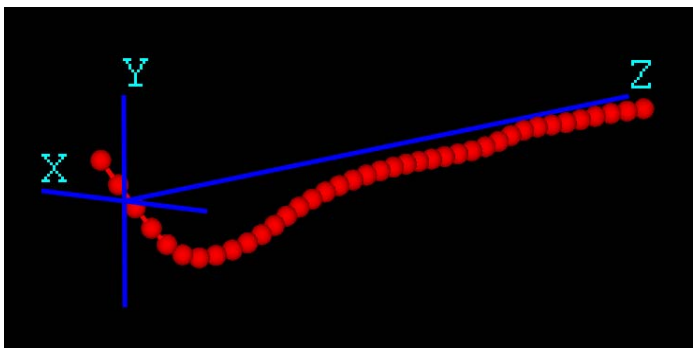

(c) 3-D vortex core profile assumed

Fig. 9 Pressure pattern (L/d_s=4.54, v/u=0.079)

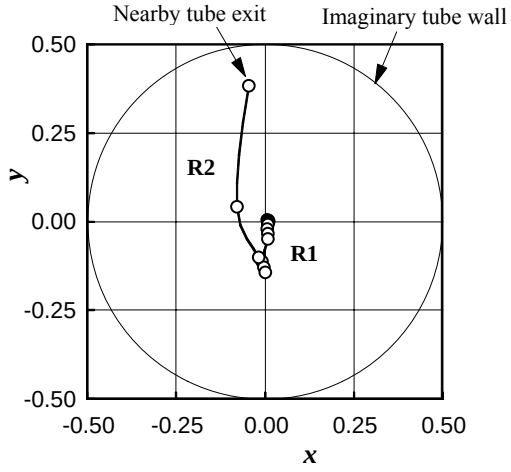

(a) Cross sectional view

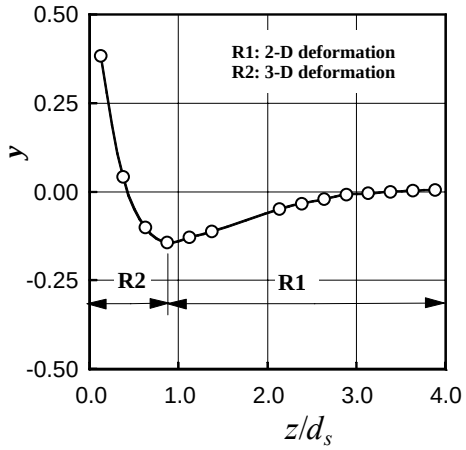

(b) Side view

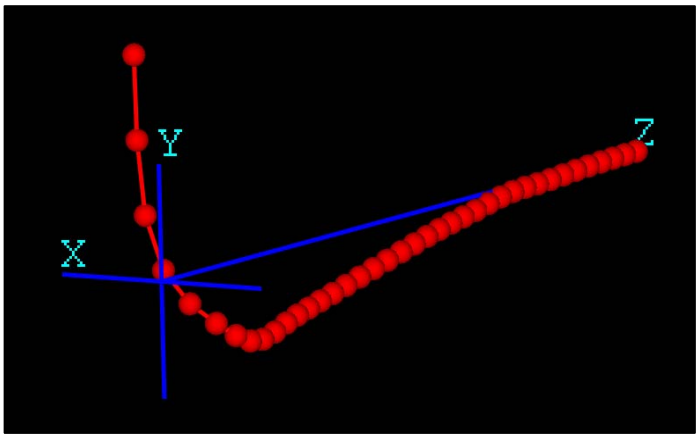

(c) 3-D vortex core profile assumed

Fig. 10 Pressure pattern (L/d_s=4.54, v/u=0.012)

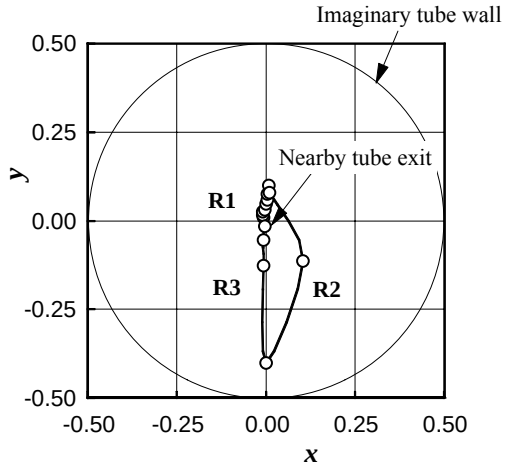

(a) Cross sectional view

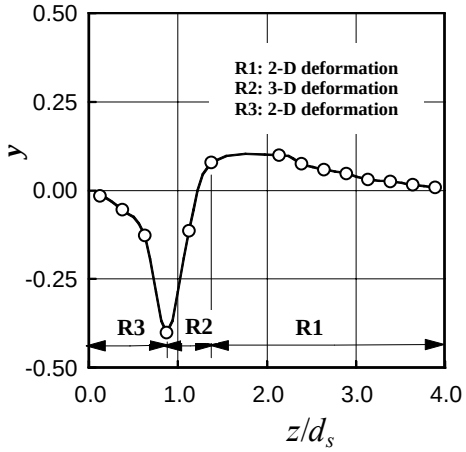

(b) Side view

Fig. 11 Pressure pattern (L/d_s=4.54, v/u=0)

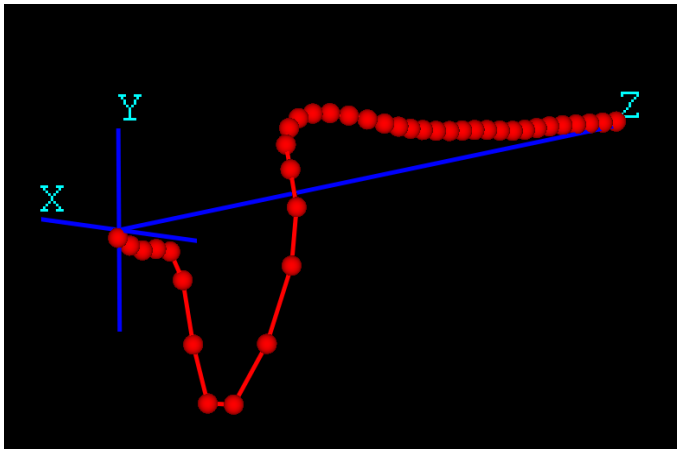

(c) 3-D vortex core profile assumed
Fig. 11 Pressure pattern (L/d_s=4.54, v/u=0)

4.5 Visualization of pressure pattern outside the tube

The measurements were carried out in order to clarify the existence of the whirling vortex in the tube. The pressure waves were measured on the disk set perpendicular to the tube axis outside the tube in which L/d_s=4.54.

Figures 12(a), 12(b), and 12(c) show the contour lines of the nondimensional pressure measured at v/u=0.079, 0.012, and 0, respectively. The region where the pressure is low represents the core of the vortex. In every case, the vortex core exists near the imaginary tube wall outside the tube. Nevertheless, the vortex core exists near the tube wall in both the case of v/u=0.079 and the case of v/u=0.012; the nondimensional pressure amplitude at v/u=0.012 is larger than that at v/u=0.079 (see Figs. 9(b) and 10(b)). The reason for this is that the concentration of vorticity is insufficient at v/u=0.079 as compared with that at v/u=0.012.

At v/u=0, the intervals of the contour lines are more uniform than those at v/u=0.079 and 0.012. This result indicates that the diffusion of vorticity is facilitated by the abrupt deformation of the vortex core (see Fig. 11(b), R2) in the tube.

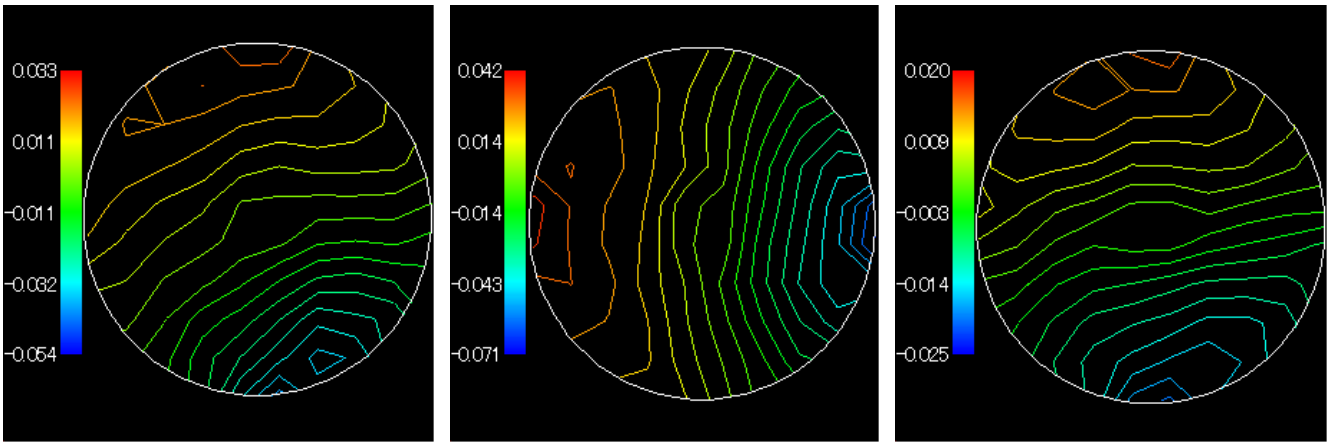

(a) v/u=0.079 **(b) v/u=0.012** **(c) v/u=0**
Fig. 12 Instantaneous counter lines of nondimensional pressure outside the tube (L/d_s=4.54)

4.6 On the type of the unsteady flow

The present study clarified that the unsteady flow due to the whirling vortex is caused in the straight tube. The occurrence of the whirling vortex has already been reported in the draft tube of the hydraulic turbine. A swirl parameter "m" was used to classify the regime of the whirling vortex in the draft tube. The parameter "m" is expressed as m=1/(v/u) by u and v used in the present study. Numerous studies on the draft tube have been carried out in the cases where m=0.7-1.8. However, the present experiment has been carried out in the cases where m>9.35. The results obtained in the draft tube could not be applied to the present study, because of the large difference in "m." As shown in Fig. 3, the present unsteady flow almost disappeared in the case where m<9.35. This finding indicates that the unsteady flow clarified in the present study differs from that measured in the draft tube. A new type of unsteady flow caused by the whirling vortex (concentration of vorticity) was found in the region where "m" has a very large value.

5. Conclusion

The main findings of this study are as follows:

Unsteady flows, mainly with 1-cell, were generated in the swirling flow in the straight tube under conditions where v/u=0.107-0.

The maximum value of the nondimensional rotational speed of the cell ($\pi d_s f_r/u$) was higher than 1.0.

The occurrence of the high-speed mode measured in the previous study (Tsurusaki, H. [1]) was confirmed in the present study.

The cause of the unsteady flows is a whirling vortex (concentration of vorticity) generated in the straight tube. The vortex core exists near the tube wall at the tube exit.

The axial distributions of the nondimensional pressure amplitude and phase differ from those suggested by the spiral vortex observed in the draft tube. Therefore, the vortex profile assumed from the measurement results is quite different from that of the spiral vortex.

A new type of unsteady flow is believed to have been found in the region where a swirl parameter "m" has a very large value (m=1/(v/u)>9.35).

Acknowledgments

The author wishes to thank Mr. Norihide Kishida, a former student of Fukuyama University, for his assistance in conducting the experiment.

Nomenclature

d_s	Inside diameter of the tube [m or mm]	u	Peripheral velocity of the inflow at $r = d_s/2$ [m/s]
f	Frequency of the pressure fluctuation [Hz]	v	Averaged axial velocity of the out flow [m/s]
f_r	Rotational speed of the cell [rps]	x	Coordinate of the vortex-core profile
L	Axial distance between the jet holes and the tube exit [m or mm]	y	Coordinate of the vortex-core profile
		z	Axial distance between the measurement point and the tube exit [m or mm]
m	Swirl parameter (u/v)		
p	Pressure amplitude [Pa]	δ	Phase lead angle of the pressure fluctuation [deg]
Q	Flow rate [m^3/s]	λ	Number of cells
r	Radius [m or mm]	ρ	Fluid density [kg/m^3]

Appendix

Frequency response of the pressure transducer

A calibration was carried out on the static characteristic of the pressure transducer used in the measurement of the frequency spectra, and a linear relationship between pressure and output voltage was obtained. In the present experiment, only the pressure fluctuations were measured by using a D.C. amplifier and an FFT analyzer. The output voltage of the D.C. amplifier (Fig. 2(a)) was in the range of about 40-520 (mV) in the present experiment. It was considered that the measured pressure amplitude was sufficiently accurate.

The natural frequency of the diaphragm of the pressure transducer is over 10 kHz. Therefore, it is considered that the output of the pressure transducer is not dependent on the frequency within the range of f<500 (Hz), where the present measurements were carried out. However, the frequency response of the pressure transducer was unclear in the case where a small pressure hole and space exist in front of the diaphragm, as shown in Fig. 1(b). The frequency response was measured using a system shown in Fig. 13. The commercial software installed in a personal computer generates a sweep signal in which the frequency gradually changes. The signal is input to the loudspeaker after amplification. The output signal of the pressure transducer mounted at a loudspeaker box is input to the computer after amplification. A frequency spectrum is obtained using the above-mentioned software. The measurement was carried out also in the case without the adapter (Fig. 14) using the same sweep signal. Figure 15 shows the variation of the pressure amplitude ratio (response in the case with the adapter /response in the case without adapter) with the frequency. The pressure amplitude ratio is within the range of 0.98-1.04. From this measurement, it was concluded that any modification was unnecessary for the measured pressure amplitude within the range of f<500 (Hz).

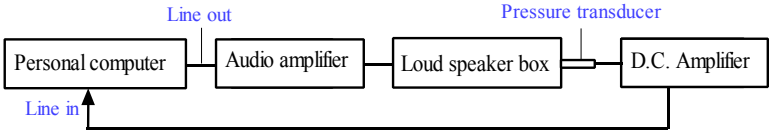

Fig. 13 Measurement system of frequency response

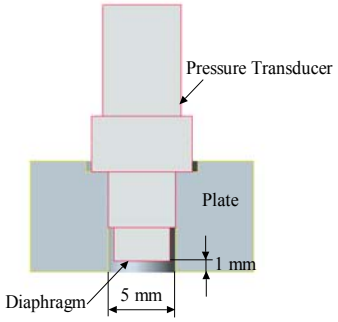

Fig. 14 Installation of pressure transducer without adapter

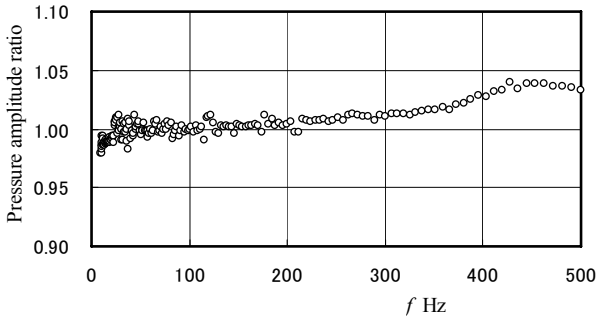

Fig. 15 Frequency response of pressure transducer with adapter (Relative value to the case without adapter)

References

[1] Tsurusaki, H., 2008, "Unsteady Flows Arising in a Mixed-Flow Vaneless Diffuser System," Int. J. Fluid Machinery and Systems, Vol. 1, No. 1, pp. 92-100.
[2] Nishi, M., et al., 1983, "Characteristics of Flow Regime and Pressure Surge of Swirl Flow in an Elbow Draft Tube," Trans. JSME, Vol. 49, No. 444, pp. 1592-1601 (in Japanese).
[3] Escudier, M., 1987, "Confined Vortices in Flow Machinery," Ann. Rev. Fluid Mech., Vol. 19, pp. 27-52.
[4] Cassidy, J. J. and Falvey, H. T., 1970, "Observations of Unsteady Flow Arising after Vortex Breakdown," J. Fluid Mech., Vol. 41, No. 4, pp. 727-736.
[5] Kurosaka, M., 1982, "Acoustic Streaming in Swirling Flow and the Ranque-Hilsch (Vortex-Tube) Effect," J. Fluid Mech., Vol. 124, pp. 139-172.